*Journal of Applied Mechanics and Technical Physics, Vol. 37, No. 3, 1996*

# STREAMWISE VORTICES IN AXISYMMETRIC JETS

N. M. Terekhova

UDC 532.526

The ideas and methods of hydrodynamic stability have proven rather fruitful for understanding of the regular features of the initial stages of transition from the laminar flow regime to the turbulent regime. In Batchelor's figurative words, it is minor reasons that lead to irreversible consequences in hydrodynamics, and hydrodynamic stability reveals weak vulnerable points in flow where random irregularities develop into typical processes of turbulent regimes.

Much attention has been traditionally concentrated on large-scale oscillations, namely, traveling waves, which are generally called the Tollmien–Schlichting waves in near-wall flows or the Rayleigh or Kelvin–Helmholtz waves in free shear flows.

However, streamwise vortex structures have been intensely studied in recent years. Such quasi-stationary waves often arise in flows both under the action of active external forces and in situations where the main flow is essentially three-dimensional. The vortices can be responsible for new transition scenarios, which are different from those previously studied, and enhance the growth of traveling waves on the local bent mean profiles created by them.

Such studies has been most successful for near-wall flows. The possibilities of the origin and development of streamwise, vortex, quasi-stationary instability in free shear layers (jet mixing layers) have been poorly studied. Recently a number of papers [1–3] have been published in which such unstable oscillations are considered for plane mixing layers.

The papers describing the characteristics, structure, and spectral composition of asimuthal irregularities for supersonic nonisobaric axisymmetric jets [4–9] are important in this respect. It has been found that a series of singularities created in free axisymmetric flow by a system of streamwise vortices can be described within the framework of the existence in it of unsteady disturbances of the Taylor–Görtler vortex type. Their origin is associated with the curvature of the gas motion trajectories under the action of centrifugal forces $\sim u^2/R_0$. Exiting from the nozzle, the gas in the compressed layer of the jet from the barrel shock (BS) to the outer jet boundary flows around the curvilinear BS boundary and is decelerated in the mixing layer. High-speed particles in the internal regions and low-speed particles in the boundary regions are affected by different centrifugal forces, which leads to additional radial azimuthal overflow of the gas. Such displacements form a system of counterrotating vortices constituting vortex pairs.

Analysis of schlieren photographs of jets presented in a number of papers (see, for instance, [10]) shows, however, that longitudinal bands identified commonly with vortices are also observed for jet regimes with very small nozzle pressure ratios and even for isobaric (optimum) jets. Such bands are typical of overexpanded jets as well. This suggests that low-intensity streamwise vortices can occur initially in free jet flows, and the nozzle pressure ratio increase, which leads to growth in the curvature $1/R_0$, only intensifies them.

The present paper describes a systematic study of the characteristics and structure of quasi-stationary vortex disturbances in axisymmetric jet flow. The simulation is carried out on the basis of numerical integration of the linearized equations of motion for an inviscid compressible nonheat-conducting gas.

The flow pattern is shown in Fig. 1, where $r$, $\varphi$, and $x$ are cylindrical variables, $v'$, $w'$, and $u'$ are the corresponding disturbance velocity components, $r_1$ and $r_2$ are the radial coordinates of the inner and outer boundaries of the mixing layer $\delta$, and $R_0$ is the radius of the jet boundary curvature, which determines the

Institute of Theoretical and Applied Mechanics, Siberian Division, Russian Academy of Sciences, Novosibirsk 630090. Translated from Prikladnaya Mekhanika i Tekhnicheskaya Fizika, Vol. 37, No. 3, pp. 45–57, May–June, 1996. Original article submitted April 11, 1995.

0021-8944/96/3703-0339 $15.00  

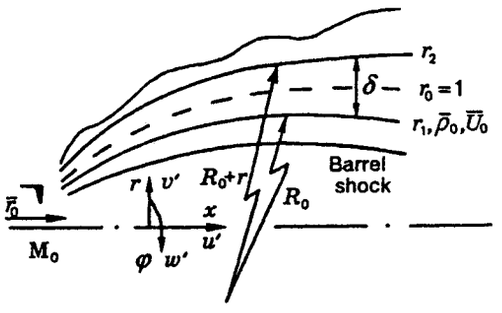


Fig. 1

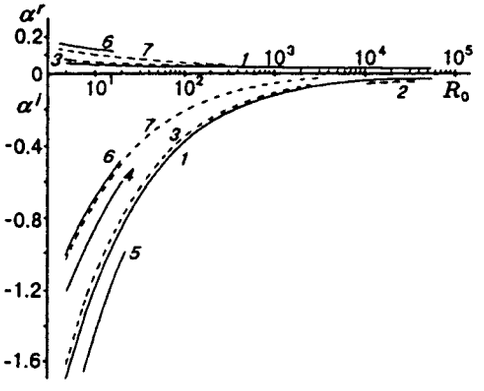


Fig. 2

active centrifugal forces. With increasing $R_0$, the flow boundaries flatten out, and in the limit $R_0 \to \infty$ the cellular structure typical of underexpanded jets with nozzle pressure ratios $N > 1$ is replaced by jet exhaust on the isobaric regime $N = 1$.

The equations are nondimensionalized to $\overline{U_0}$ and $\bar{\rho}_0$ (at the inner boundary for $r = r_1$) and to the value of $\bar{r}_0$ for which $\overline{U}/\overline{U}_0 = 0.5$. For an isobaric jet, $\bar{r}_0$ coincides with the nozzle radius, and generally $r_1 = 1 - \delta/2$ and $r_2 \gtrsim 1 + \delta/2$. One-dimensional mean flow has the following representation for the axial velocity:

$$U(r) = \begin{cases} 1, & r < r_1, \\ \exp(-b\eta^2), & r \geqslant r_1. \end{cases} \tag{1}$$

Here $\eta = 2(r - r_1)/\delta$, $b = \ln 2$, and $U'(r) = -4b\eta U/\delta$. The mean density $\rho_0$ is related to $U$ through the gasdynamic relation

$$\rho_0 = [1 + (æ - 1)\,\mathrm{M}_0^2\,(1 - U^2)/2]^{-1}, \tag{2}$$

and the speed of sound $a = (\rho_0 \mathrm{M}_0^2)^{-1/2}$ ($\mathrm{M}_0$ is the Mach number at the nozzle exit).

The equations of motion with active centrifugal forces for axisymmetric flow (Fig. 1) were derived in [4]. Let us define the vortex disturbances as

$$v',\, u',\, p',\, \rho' = (i\hat{v}, \hat{u}, \hat{p}, \hat{\rho})\,(r)\,\mathrm{e}^{i\theta}\cos n\varphi, \quad w' = i\hat{w}\,(r)\,\mathrm{e}^{i\theta}\sin n\varphi, \quad \theta = \alpha x - \omega t, \tag{3}$$

where $\rho'$ and $p'$ are the density and pressure disturbances; $\omega$ is the angular frequency; $\alpha = \alpha^r + i\alpha^i$; $\alpha^r$ and $n$ are the longitudinal and azimuthal wavenumbers; and $\alpha^i$ is the longitudinal wave amplification factor. The value of $n$ defines the number of vortex pairs along the circle of the flow field: small $n$ correspond to large-scale vortices and large $n$, to small-scale ones.

The linearized equations for the pressure disturbance amplitude $\hat{p}$ are written as

$$\hat{p}'' + A_1\hat{p}' + A_2\hat{p} = -\{[1 + \alpha U/F + A_3]\,\hat{p}' + [(1/R_0 + U'/U + A_1 + A_3)\,2\alpha U/F - (A_2 + \alpha^2)\,B/F^2]\,\hat{p}\}/R_0,$$
$$(') = d/dr, \qquad F = \alpha U - \omega, \quad F_1 = F^2 - B/R_0, \qquad B = 2U\,(U' + U/R_0), \tag{4}$$
$$A_1 = 1/r - \rho_0'/\rho_0 - 2F'/F, \quad A_2 = F^2/a^2 - n^2/r^2 - \alpha^2, \quad A_3 = (B' - 2BF'/F)/F_1, \quad |\hat{p}|_{\max} = 1$$

with the boundary conditions $\hat{p} \to 0$ outside $\delta$ for $r < r_1$ and $r > r_2$ [4, 6]. Additional terms associated with centrifugal forces are written on the right-hand side of (4). The amplitude functions of disturbances are found from the system

$$\hat{v} = (F\hat{p}' + 2\alpha U\hat{p}/R_0)/\rho_0 F_1, \quad \hat{w} = -n\hat{p}/r\rho_0 F, \quad \hat{u} = -[(U' + U/R_0)\,\hat{p}' + \alpha F\hat{p}]/\rho_0 F_1, \quad \hat{\rho} = \hat{p}/a^2 - \rho_0'\hat{v}/F. \tag{5}$$

The real parts of Eqs. (3) and (5) define the physical components of wave velocities and density:

$$v' = v\,(r)\exp(-\alpha^i x)\cos n\varphi, \quad v = -\hat{v}^r \sin\theta_1 - \hat{v}^i \cos\theta_1,$$

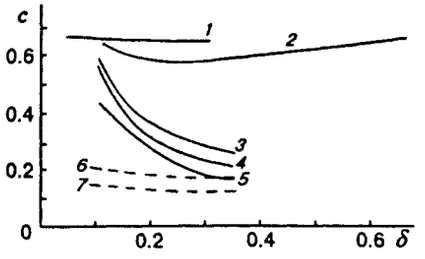


Fig. 3

$$u' = u(r)\exp(-\alpha^i x)\cos n\varphi, \quad u = \hat{u}^r \cos\theta_1 - \hat{u}^i \sin\theta_1, \quad \theta_1 = \mathrm{Re}(\theta).$$

Disturbances with $\omega \to 0$ are considered, which corresponds to a small value of the acoustic Strouhal number (or Helmholtz number) Sr = 0.005, the time period of the wave being $T_t \sim 250$.

Figure 2 shows the eigenvalues of $\alpha^r$ and $\alpha^i$ within a wide range of $R_0$ ($5 \leqslant R_0 \leqslant 3 \cdot 10^4$) for several regimes with mixing layer thickness $\delta = 0.2$. The basic regime is the one with $M_0$=1.5 for the azimuthal mode $n = 16$ (curve 1).

We now consider sequentially the results of numerical simulation of this regime with respect to $R_0$ value variation.

*Limiting Large Values of* $R_0$ ($R_0 > 10^4$). In the limit $R_0 \to \infty$, this case can be correlated with the isobaric flow regime in which no trajectory curvature is observed. It is seen from Fig. 2 that the values of increments of $\alpha^i$ are rather small and decrease only slightly with growing $R_0$. The wavenumbers $\alpha^r$ of disturbances are thereat nearly constant ($\alpha^r \sim 0.0375$), which corresponds to wavelengths $\lambda \sim 170\bar{r}_0$, and the phase velocities $c = \omega/\alpha^r$ are constant ($c \sim 0.67$) for all $\delta$ under consideration. Figure 3 (curve 1) illustrates this fact for $R_0 = 2 \cdot 10^4$. This weak variation of the disturbance parameters suggests that such quasi-stationary waves are typical of a free isobaric axisymmetric jet for $M_0$= 1.5. Because of the inviscid nature of the governing equations (4) we have to restrict consideration only to these limiting cases, since further increase in $R_0$ accompanied by reduction of $\alpha^i$ is not possible, because of errors arising in regions $U \sim 0$.

We consider the vector field of velocities $v'$ and $w'$ for various values of $\delta$. Such configurations give an idea of the shape of streamwise vortices in various downstream $x$ cross-sections. In what follows, we shall not specify the dependence $x(\delta)$, assuming the thickness $\delta$ to be a scale parameter. The radial distributions of wave velocities for $R_0 = 2 \cdot 10^4$ are presented in Figs. 4a–4c for $\delta = 0.05$, 0.1, 0.125, and 0.15 (curves 1–4, respectively). They were computed on the basis of (4). The values of $v'$ and $w'$ make it possible to present the sequence of downstream changes of vortex configurations. Only one vortex in the interval $0 \leqslant n\varphi \leqslant \pi$ is shown in Fig. 4d. The second vortex of this pair in the interval $\pi \leqslant n\varphi \leqslant 2\pi$ is symmetric to the vortex shown in the figure and is counterrotating. Figure 4e shows the downstream evolution of a vortex pair for the mode $n = 16$.

For small $\delta$ values, a vortex pair with an approximately equal ratio of azimuthal and radial motion is formed near the nozzle exit in the near-root region. The center of the vortex is close to the coordinate $|U'|_{\max}$. Advection swirls the vortices in this pair so that the right- and left-rotating vortices, in overlapping, change places to form a vortex core. The azimuthal overflow is enhanced, and the radial overflow decreases considerably. Further downstream the vortex orientation does not change.

This dynamics is observed for all disturbances for $R_0 > 10^4$. The dashed curves in Figs. 4a–4c show the velocity distributions for $R_0 = 27300$. It is seen that a further increase in the radius $R_0$ has practically no effect on the wave velocity shape or values. Variations in the streamwise component $u$ completely correlate with variations in the radial velocity $v$ direction. Positive values of $v$ (overflow from the vortex core to the flow periphery) are accompanied by the mass entrainment of high-speed gas and correspond to positive values of $u$, while a change in the radial motion direction (introduction of low-velocity mass from external regions)

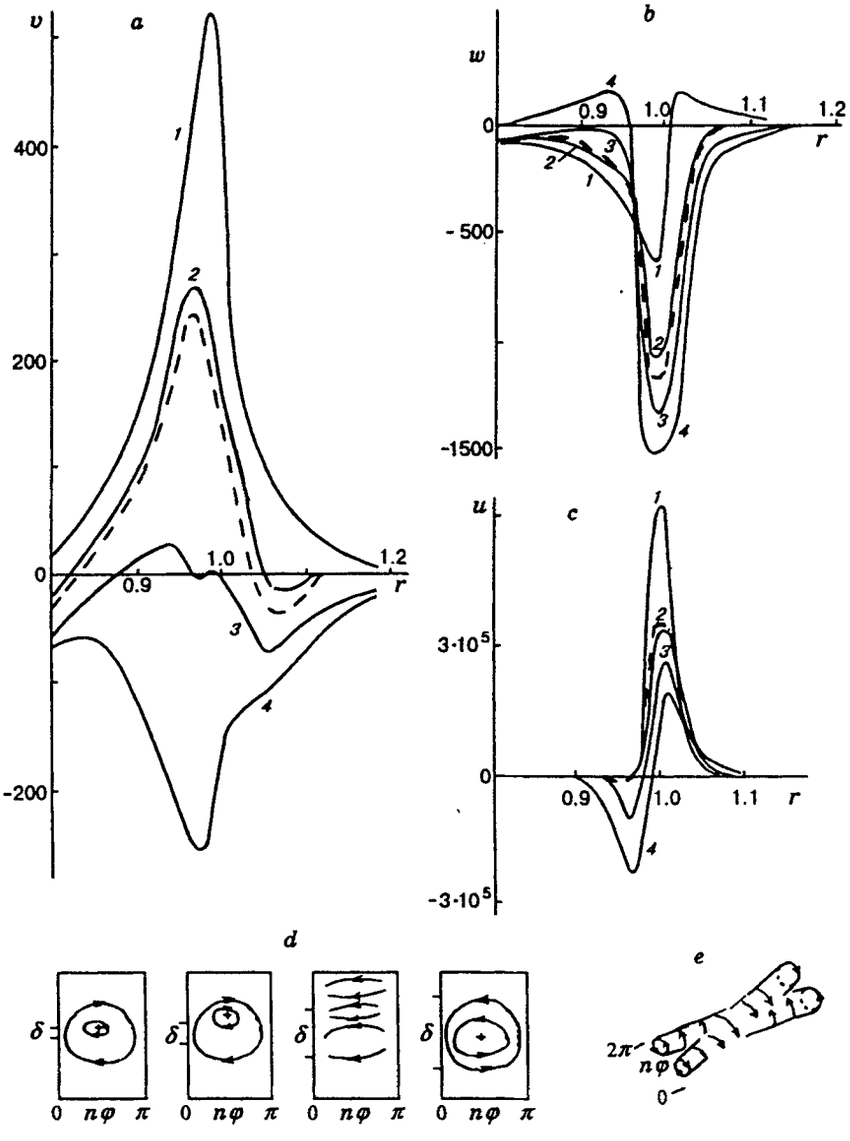


Fig. 4

is accompanied by the appearance of negative $u$ and an appreciable relative decrease in the positive values.

It was found that with increasing $R_0$ within the range of these limiting values, the swirl step of the vortex core is reduced, i.e., swirling is shifted closer to the jet root to the region of very small $\delta$. We were unable to study the range of $\delta > 0.25$ in all variants. Such core formation in vortex pairs is typical of very large $R_0$ and is determined by shear forces (mean motion gradients) that form the profile. Increasing centrifugal forces lead to a change of disturbed motion shape.

*Large Values of* $R_0$ ($200 < R_0 < 10^4$). Let as consider in more detail the variant of $R_0 = 5 \cdot 10^3$, for which the region of $0.05 \leqslant \delta \leqslant 0.65$ was calculated. The longitudinal increments are still small (see Fig. 2); their downstream variation and longitudinal wavenumber values $\alpha^r$ are shown in Fig. 5. As the jet propagates downstream, the increments $\alpha^i$ are reduced, which is typical of all regimes, whereas the values of $\alpha^r$ are fairly stable.

Vortex configurations for various $\delta$ are shown in Figs. 6a–6c (curves 1–6 represent $\delta = 0.1$, 0.2, 0.3, 0.4, 0.5, and 0.6, respectively). The vortex shape and orientation in the near-root region ($\delta < 0.15$) are the

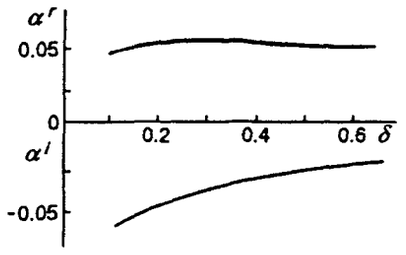


Fig. 5

same as for the limiting $R_0$, but downstream core formation is replaced by expulsion of the initial vortex into the external region. The expulsion results in the formation of another vortex in the high-velocity region. This vortex is counterrotating with respect to the initial one, and a vortex pair exists in the crossflow region of the mixing layer. The phase velocity of the wave decreases thereat, as is seen from Fig. 3 (curve 2). The downstream jet propagation leads to complete deceleration and vanishing of the initial vortex, and the second vortex dominates in the interval $0.3 \leqslant \delta \leqslant 0.45$. The process is then repeated: another counterrotating vortex arises in the internal region, and at $\delta > 0.45$ a vortex pair is again observed. The mean gradients in this region are not high ($|U'|_{\max} \sim 2.5$), and no expulsion occurs. The center of the already existing vortex occupies a position near $r \sim 0.95$, whereas the center of the second vortex is shifted toward it from internal regions. The phase velocity of the wave starts to increase (see Fig. 3).

The crossflow distributions of the axial velocity $u$ reflect the reconstruction of the vortex pattern, which is accompanied by a reduction of the level of $u > 0$ at high $r$, by the appearance of regions of negative axial velocities, and, finally, by establishment of distributions with three local maxima for large $\delta$ (Fig. 6d).

As the centrifugal forces increase, at least up to $R_0 > 200$, no qualitative changes in the vortex configurations take place. One can only note an increase in the region of existence of the initial single vortex. Thus, for $R_0 = 5 \cdot 10^3$ this region is bounded by $\delta \sim 0.15$, whereas for $R_0 = 0.5 \cdot 10^3$ the interval is extended up to $\delta \sim 0.35$ and for $R_0 = 0.2 \cdot 10^3$ up to $\delta \sim 0.5$.

*Moderate Values of $R_0$.* For $50 \leqslant R_0 \leqslant 200$, one can again note vortex-core formation in the region of small $\delta$, as in the above-described cases. This is illustrated in Fig. 7 for $\delta = 0.1$, 0.16, 0.18, and 0.2 (curves 1–4) at $R_0 = 50$. In the initial vortex, whose center is in the region of low flow velocities ($U \sim 0.01$) outside the conventional outer boundary of the mixing layer $r_2$, downstream jet propagation leads to change of the sign of the radial component $v$, which should be interpreted as the onset of core formation in the pair in the interval $0 \leqslant n\varphi \leqslant 2\pi$. For $\delta > 0.2$, the entire crossflow region of the mixing layer is occupied by a single vortex, which is counterrotating with respect to the near-root vortex. The values of $v$ and $w$ are of the same order there, and the center of this second vortex is close to the middle of the mixing layer and is shifted toward the outer boundary during downstream jet propagation. Note that though the maximum values of $v$, $w$, and $u$ are within the mixing layer, the radial and azimuthal components outside the layer $\delta$ decay asymptotically, propagating rather deeply both in the flooded near-jet space and in the region adjacent to the inner boundary of the mixing layer. The longitudinal component $u$ is absent in this region. The phase velocity of the wave for $R_0 = 50$ is shown by curve 3 in Fig. 3; its reduction with growth in $\delta$ is observed. The increments of $\alpha^i$ for such moderate $R_0$ increase by an order of magnitude compared with the values for high $R_0$.

Evidently, for $R_0 < 50$, the governing forces will be centrifugal forces. Precisely for such $R_0$ one can regard the streamwise vortex disturbances as Taylor–Görtler waves.

*Small Values of $R_0$. Taylor–Görtler Waves.* The longitudinal increments of $\alpha^i$ increase considerably for disturbances for $R_0 < 50$ (see Fig. 2). Precisely these $R_0$ values are observed in nonisobaric underexpanded jets at $N > 1$. The features of Taylor–Görtler waves have been thoroughly studied by Zheltukhin et al. [4–7].

It was found that an increase in centrifugal forces (reduction in $R_0$) leads to vortex localization in the mixing layer for small $R_0$ compared with its moderate values, and the downstream dynamics involves gradual expulsion of the vortex into the external region, the process being attenuated by $R_0$ reduction. It

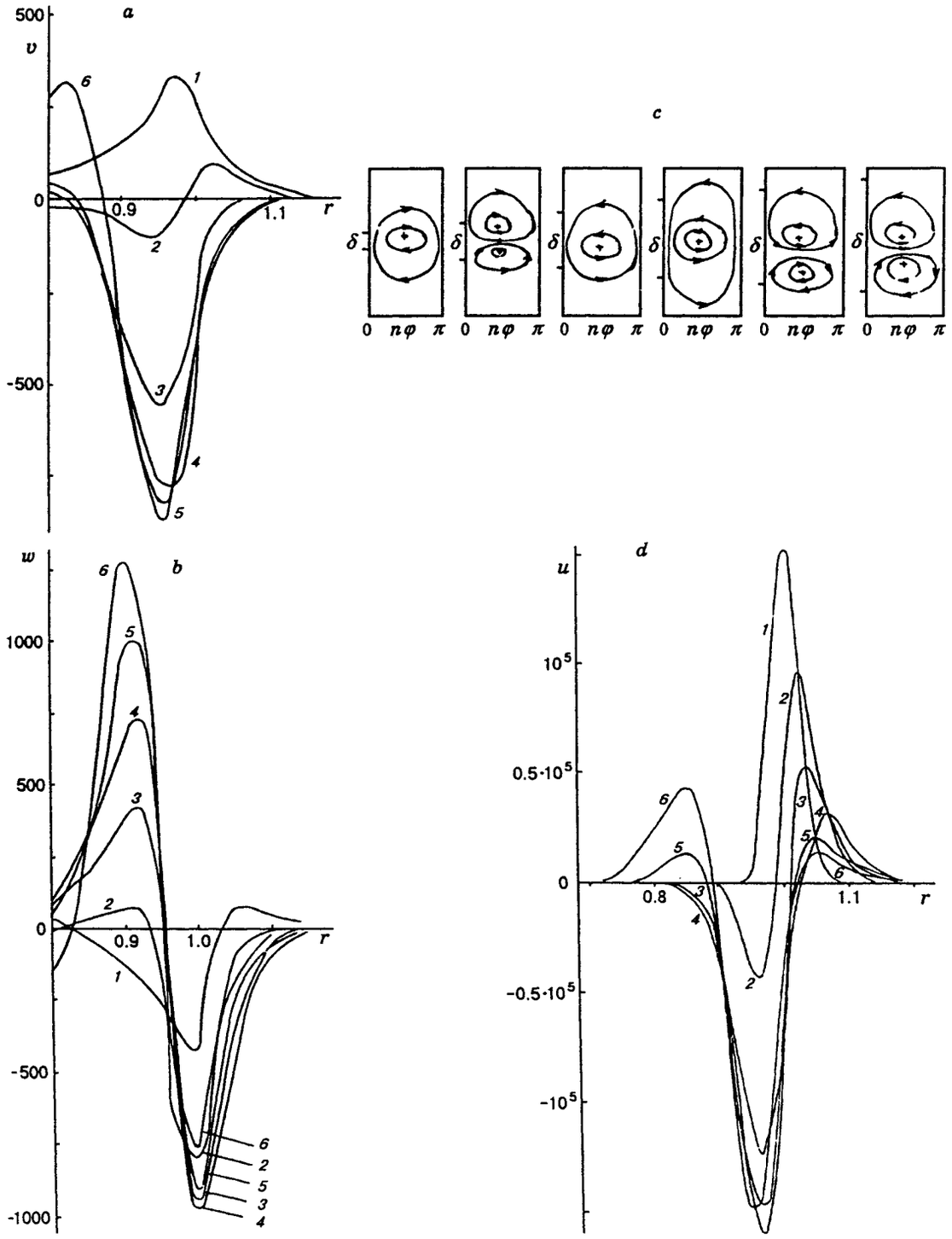
a
v
500
0
-500
0.9
1.1
r
1
2
3
4
5
6
c
δ
0
nφ
π
b
w
1000
500
-1000
1.0
d
u
10^5
0.5·10^5
-0.5·10^5
-10^5
0.8

Fig. 6

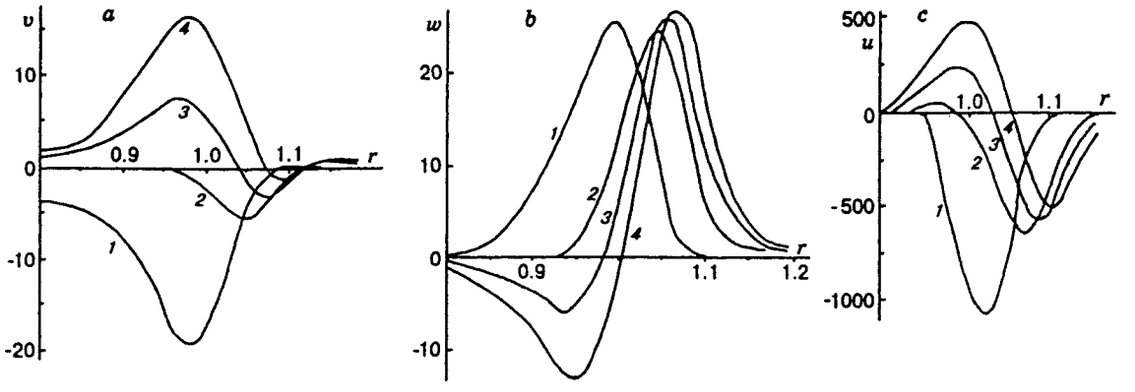


Fig. 7

seems reasonable to discuss typical distributions of the wave velocities $v$, $w$, $u$, and $\delta p_0$ for $R_0 = 20$ and 5.

The downstream reconstruction of the vortex pattern for $R_0 = 20$ (Fig. 8) shows that in the initial near-root vortex with the same order of $v$ and $w$ the radial component is considerably reduced and the azimuthal one increases. Thus, gas particles in the external regions begin to move along nearly circular trajectories as if they flow around the second counterrotating vortex that has originated near the inner boundaries with considerable radial motion. The center of the second vortex is gradually shifted from the inner boundaries to the center of the layer $\delta$ and then to the outer boundary. Curves 1–4 correspond to $\delta = 0.1$, 0.2, 0.3, and 0.35.

The crossflow distributions of $|u|$ acquire a typical shape with two peaks. As $\delta$ increases, the first peak shifts to the region of large $r$ and decreases, while the value of the second peak increases in the region $r \sim 1$. The appearance of these typical distributions of the axial component leads to qualitative reconstruction of the crossflow distributions of the total pressure variations $\delta p_0$, which are described by the following relation [4, 6] with accuracy up to quadratic terms:

$$\delta p_0 = p_0 \left[ \left( \frac{æ - 1}{æ} \frac{p'}{p_j} + \frac{2u'}{U} \right) \frac{æ \mathrm{M}^2}{2 + (æ - 1)\mathrm{M}^2} + \frac{p'}{p_j} \right], \quad \mathrm{M} = \frac{U}{a}.$$

Special attention should be paid to the character of the $\delta p_0$ distributions, because this quantity has been measured in experiments [5, 8, 9] and compared with computations. The character of $\delta p_0$ evolution determines the axial increments of $\alpha^i$, and therefore, ignoring these features can give rise to high errors in $\alpha^i$ values. It is also important to determine the value of $R_0$ very accurately. Equation (4) used for simulation is obtained under the assumption of the local constancy of $R_0$, and in further research one should try to take into account the dependence $R_0(x)$ or $R_0(\delta)$, which could be done by direct numerical integration of linearized equations of motion by finite-difference methods.

In the present paper, the author made no attempt at criterial description of the acting forces by means of Görtler or Richardson numbers, since this would only hamper understanding, because of the absence of a clear notion of the dependences on some easily representable quantities.

For $R_0 = 5$, distributions could be obtained only for $\delta \lesssim 0.33$; they are shown in Fig. 9 for $\delta = 0.1$–$0.3$ (curves 1–3). For these values of $\delta$, a single vortex is formed in the mixing layer, and its center is gradually shifted from the middle of the layer ($r \sim 1$) toward the outer boundary. The ratios of $v$ and $w$ are approximately equal there; both components grow downstream, just as the axial component $u$. The maximum of $|u|$ shifts from the middle of the layer to the outer boundary, and again a considerable change in $\delta p_0$ in the cross-section is observed, although there are no sharp changes in $\delta p_0$ for this configuration, which is simpler than the configuration for $R_0 = 20$.

The overall intensity of the transverse azimuthal overflow increases. Thus, the ratios $v/u$ and $w/u$ vary from 0.088 for $\delta = 0.1$ to 0.122 for $\delta = 0.3$. The phase velocity for $R_0 = 20$ corresponds to curve 4, and for $R_0 = 5$, to curve 5 in Fig. 3. Until now we discussed only the shape and values of the wave velocities of

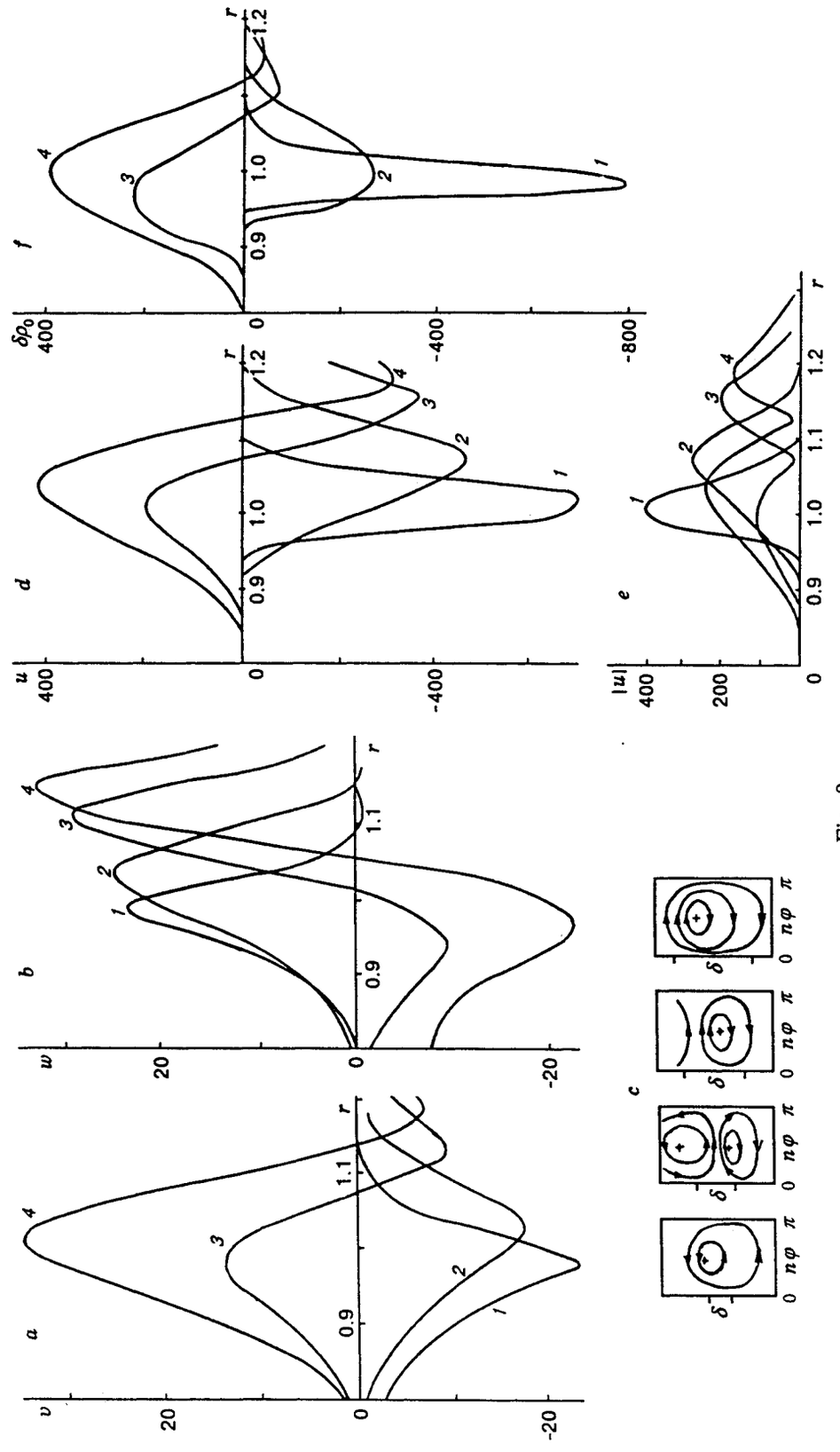


Fig. 8

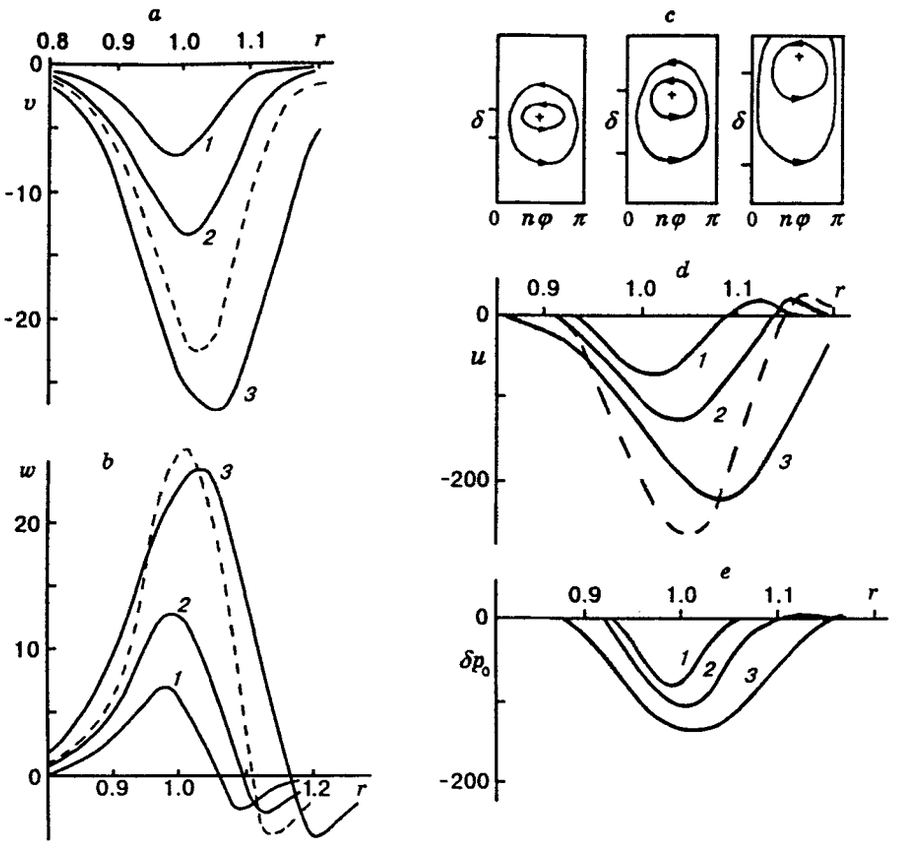


Fig. 9

disturbances; therefore, it seems reasonable to give crossflow distributions of the wave density. They are shown in Figs. 10 and 11 for $R_0 = 20$ and 5, respectively, for $n\varphi = 0$ (the notation is the same as in Figs. 8 and 9). On the whole, these distributions correlate well with the character of $u$. Thus, the addition of low-speed mass with moderate mean density from external regions corresponds to $\rho < 0$ and leads to reduction in the mean local values. The mass entrainment from internal regions corresponds to $\rho > 0$ and hence is responsible for their increase. The maximum of $\rho$ in $\rho(r)$ distributions is displaced to higher mean flow velocities, as compared with localization of $|u|_{\max}$.

*Other Spectral Modes.* Vortex shapes for modes $n = 8$ and 24 are quite well studied. Figure 2 shows the increments of these modes for the same calculation parameters ($M_0$=1.5 and $\delta = 0.2$, curves 4 and 5, respectively). They support the regularity that was already noted in [4, 6], namely, small-scale waves with large azimuthal numbers are more unstable.

Examination of the evolution of the vortex disturbances shows that it agrees well with the stages described in detail for mode $n = 16$. Therefore, without going into details, we note some distinctive features and general tendencies found in such comparative analysis for small $R_0$ at large values of centrifugal forces ($R_0 < 50$).

(1) In the near-root region for small $\delta$, an increase in the mode number is accompanied by more expressed vortex localization in the mixing layer. For $R_0 = 5$ and $\delta = 0.15$, its center is determined by the coordinate $r = 1.09$, 1.06, and 1.03 for $n = 8$, 16, and 24.

(2) Vortex expulsion into the external region is delayed. Coincidence of the center of the vortex with the conventional outer boundary $r_2$ is confirmed by the following data: $\delta = 0.12$, 0.2, and 0.25 for $n = 8$, 16, and 24.

(3) With increasing $n$ for moderate $R_0$ the second counterrotating vortex near the inner boundaries

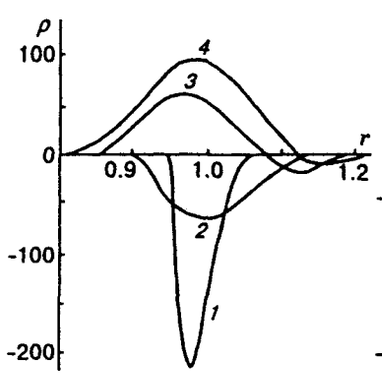

Fig. 10

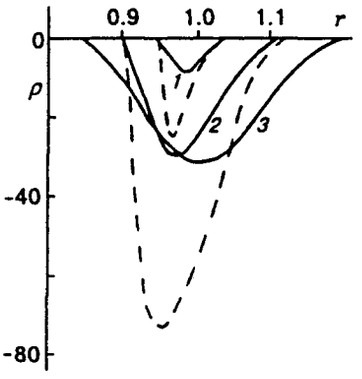

Fig. 11

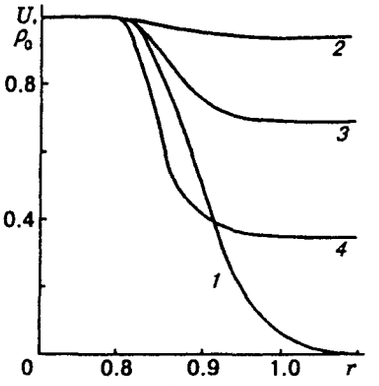

Fig. 12

appears sooner. For $R_0 = 20$, this process is related to $\delta = 0.33$, 0.225, and 0.18 for $n = 8$, 16, and 24.

(4) It is difficult to find a criterion that determines vortex motion intensity because of the above-mentioned reconstruction of vortex configurations. Note that azimuthal overflow always increases downstream.

*Efflux Mach Number Effect.* The principal question here is that of the compressibility effect on such quasi-stationary disturbances. Changes in the crossflow distributions of the mean density $\rho_0(r)$ and speed of sound $a(r)$ entering the basic linearized equation (4) are known to be associated with efflux Mach number variation. Growth in $M_0$ produces an increase in relative differences in distributions $\rho_0(r)$ and gradients $\rho_0'$. As a consequence, the question arises of whether the disturbances considered are an integral part of compressible flows or are inherent in axisymmetric shear flows. Note that such disturbances have been found for plane mixing layers at least numerically [1, 3]. Novopashin and Perepelkin [11, 12] found experimentally the presence of azimuthal inhomogeneities in the density distribution in a transitional supersonic low-density jet. They associate the nature of this ingomogeneity with instability due to the spread in density, which is noted as the predominant factor.

The present work included test calculations for $M_0 = 3$ and 0.5. From relation (2) follow the distributions $\rho_0(r)$ shown in Fig. 12 for $\delta = 0.4$ and $M_0 = 0.5$, 1.5, and 3 (curves 2–4). Curve 1 shows the mean velocity $U$ calculated from formula (1). As is seen, the relative difference in $\rho_0$ for $M_0 = 0.5$, 1.5, and 3 amounts to 5, 31, and 64.4%, respectively. However, such density gradients across $\delta$ affect $\alpha^i$ rather weakly (curves 2 and 3 for $M_0 = 0.5$ and 3 in Fig. 2). For the $R_0$ examined, the disturbances for large $M_0$ values are more stable, which is also typical for traveling shear instability waves, i.e., compressibility is a stabilizing factor, and higher-speed jets have an elevated stability factor, which prevents growth of small disturbances in the mixing layer. Note that the wavenumbers $\alpha^r$ increase only slightly with growing $M_0$ (curve 3 for $M_0 = 3$ in Fig. 2).

The wave velocity distributions for $M_0 = 3$ for $n = 16$ agree well the distributions for $M_0 = 1.5$ and are shown by dashed curves for $\delta = 0.2$ in Fig. 9 for $R_0 = 5$ (cf. curve 2). Higher velocity values are worthy of notice but their ratios remain principally the same. Growth in the wave density (dashed curves in Fig. 11) is noted in the same proportion.

These distributions indicate that a Mach number increase has practically no effect on the vortex configuration patterns.

The presence of terms in (4) related to compressibility causes the appearance of additional eigenvalues of $\alpha$ and eigensolutions of the form of (3) and (5), which also satisfy the boundary-value problem for eigenvalues. This peculiar feature is inherent in compressible boundary layers and is well systematized in [13] using traveling waves as an example. An additional branch of such a solution was found in the present work, and the wave shapes of the second mode were obtained.

Curves 6 and 7 in Fig. 2 show the dependences $\alpha(R_0)$ for waves with $n = 16$ for $M_0 = 1.5$ and 3, respectively. The increment values are fairly close, but the disturbances for higher Mach numbers are found for the first time to be more unstable. The wavenumbers of these disturbances are higher than for the first

mode.

The wavelength for $M_0 = 1.5$ decreases by a factor of 4 and that for $M_0 = 3$, by a factor of 1.5. The phase velocities for $M_0 = 1.5$ are shown in Fig. 3 by curves 6 and 7 at $R_0 = 20$ and 5, respectively. Note their conservatism compared with the first mode.

The vortex configurations become more complex. As a rule, in the crossflow region of the mixing layer two counterrotating vortices are present immediately in the near-root region of the jet. Vortex core formation is observed, and the stable coexistence of the vortex pair takes place downstream for both high and low $\delta$.

A detailed analysis of all features of vortex evolution makes no sense for two reasons. First, since waves of the second mode have smaller increments, they are more stable and grow less intensely in space. Second, the existence of simple forms of disturbed motion, which are inherent in disturbances of the first mode, is more probable in flow under natural regulation. But information on the possible occurrence of such disturbances in free axisymmetric supersonic flow is certainly necessary for gasdynamicists, and experimenters should take into account this ambiguity in interpreting experimental results.

Despite its purely descriptive character, the investigation performed can fill the vacuum that always accompanies the study of a new phenomenon, thus creating an information field that can be analyzed and refined, as necessary. Thus, the simulation performed confirmed the possibility of existence of streamwise vortex instability in free axisymmetric jet flow.

## REFERENCES


1. M. E. Goldstein and J. Mathew, "The development of a mixing layer under the action of weak streamwise vortices," *Phys. Fluids, A*, **5**, No. 3, 600–607 (1993).
2. J. A. K. Stott and P. W. Duck, "The stability of a trailing-line vortex in compressible flow," *J. Fluid Mech.*, **269**, 323–351 (1994).
3. W. W. Liou, "Linear instability of curved free shear layers," *Phys. Fluids*, **6**, No. 2, 541–549 (1994).
4. N. A. Zheltukhin and N. M. Terekhova, "Disturbances of high modes in a supersonic jet," *Zh. Prikl. Mekh. Tekh. Fiz.*, No. 2, 75–83 (1990).
5. N. A. Zheltukhin, V. I. Zapryagaev, A. V. Solotchin, and N. M. Terekhova, "Spectral composition and structure of Taylor–Görtler vortices in a supersonic underexpanded jet," *Dokl. Ross. Akad. Nauk*, **325**, No. 6, 1133–1137 (1992).
6. N. A. Zheltukhin and N. M. Terekhova, "Taylor–Görtler instability in a supersonic jet," *Prikl. Mekh. Tekh. Fiz.*, **34**, No. 5, 48–55 (1993).
7. N. A. Zheltukhin and N. M. Terekhova, "Modeling of stationary longitudinal vorticity in the initial section of supersonic jet," in: Proc. of the Int. Conf. of the Methods of Aerophysical Research, Novosibirsk, Part 2 (1992).
8. V. I. Zapryagaev and A. V. Solotchin, "Three-dimensional flow structure in a supersonic underexpanded jet," *Zh. Prikl. Mekh. Tekh. Fiz.*, **34**, No. 4, 42–47 (1991).
9. V. I. Zapryagaev, S. G. Mironov, and A. V. Solotchin, "Spectral composition of wave numbers of longitudinal vortices and characteristics of flow structure in a supersonic jet," *Prikl. Mekh. Tekh. Fiz.*, **34**, No. 5, 41–47 (1993).
10. P. J. Lamont and B. L. Hunt, "The impingement of underexpanded axisymmetric jets on wedges," *J. Fluid Mech.*, **76**, 307–336 (1976).
11. S. A. Novopashin and A. L. Perepelkin, "Flow self-organization in a supersonic preturbulent jet," Preprint No. 175–88, Inst. of Thermophysics, Sib. Div., Russian Acad. of Sciences, Novosibirsk (1988).
12. S. A. Novopashin and A. L. Perepelkin, "Origin and development of turbulence in a strongly underexpanded jet," *Sib. Fiz.-Tekh. Zh.*, No. 1, 89–96 (1991).
13. S. A. Gaponov and A. A. Maslov, *Development of Disturbances in Compressible Flows* [in Russian], Nauka, Novosibirsk (1980).